INTERFACE FOCUS

rsfs.royalsocietypublishing.org

Research

Cite this article: Sacks MS, Zhang W, Wognum S. 2016 A novel fibre-ensemble level constitutive model for exogenous cross-linked collagenous tissues. *Interface Focus* **6**: 20150090.
http://dx.doi.org/10.1098/rsfs.2015.0090

One contribution of 19 to a theme issue 'Integrated multiscale biomaterials experiment and modelling: towards function and pathology'.

Subject Areas:
bioengineering, biomechanics

Keywords:
collagenous tissues, cross-linking, constitutive model

Author for correspondence:
Michael S. Sacks
e-mail: msacks@ices.utexas.edu

THE ROYAL SOCIETY PUBLISHING

A novel fibre-ensemble level constitutive model for exogenous cross-linked collagenous tissues

Michael S. Sacks[1], Will Zhang[1] and Silvia Wognum[2]

[1]Center for Cardiovascular Simulation, Institute for Computational Engineering and Sciences, Department of Biomedical Engineering, The University of Texas at Austin, 201 East 24th Street, PO Box 5.236, Stop C0200, Austin, TX 78712, USA
[2]Department of Biomedical Engineering, Eindhoven University of Technology, PO Box 513, 5600 MB Eindhoven, The Netherlands

WZ, 0000-0003-1986-6253

Exogenous cross-linking of soft collagenous tissues is a common method for biomaterial development and medical therapies. To enable improved applications through computational methods, physically realistic constitutive models are required. Yet, despite decades of research, development and clinical use, no such model exists. In this study, we develop the first rigorous full structural model (i.e. explicitly incorporating various features of the collagen fibre architecture) for exogenously cross-linked soft tissues. This was made possible, in-part, with the use of native to cross-linked matched experimental datasets and an extension to the collagenous structural constitutive model so that the uncross-linked collagen fibre responses could be mapped to the cross-linked configuration. This allowed us to separate the effects of cross-linking from kinematic changes induced in the cross-linking process, which in turn allowed the non-fibrous tissue matrix component and the interaction effects to be identified. It was determined that the matrix could be modelled as an isotropic material using a modified Yeoh model. The most novel findings of this study were that: (i) the effective collagen fibre modulus was unaffected by cross-linking and (ii) fibre-ensemble interactions played a large role in stress development, often dominating the total tissue response (depending on the stress component and loading path considered). An important utility of the present model is its ability to separate the effects of exogenous cross-linking on the fibres from changes due to the matrix. Applications of this approach include the utilization in the design of novel chemical treatments to produce specific mechanical responses and the study of fatigue damage in bioprosthetic heart valve biomaterials.

1. Introduction

The application of exogenous-cross-links (EXLs) to native or biologically derived soft collagenous tissues finds its way into a wide range of medical therapies and device applications, such as surgical biomaterials, modification of corneal tissues (using riboflavin/UVA) and vascular grafts. Perhaps the most mechanically demanding application is the so-called bioprosthetic heart valve (BHV), which is fabricated from several types of biologically derived soft collagenous tissue membranes. From a clinical perspective, BHVs have important advantages in that they do not require permanent anticoagulation therapy, operate noiselessly, and have blood flow characteristics similar to the native valve, and thus have become the dominant heart valve therapy worldwide [1–3]. However, BHV durability continues to remain limited to the range of 10–15 years, resulting from leaflet structural deterioration mediated by fatigue and/or tissue mineralization [4,5]. In general, structural damage is a critical factor in BHV degeneration, and clearly implicates coupled material and design factors as major limiters to long-term durability [6,7]. However, a major reason why advances in the use of cross-linked tissues in BHVs and other biomedical applications is a dearth of knowledge on how EXLs affect the underlying tissue structure and macroscopic

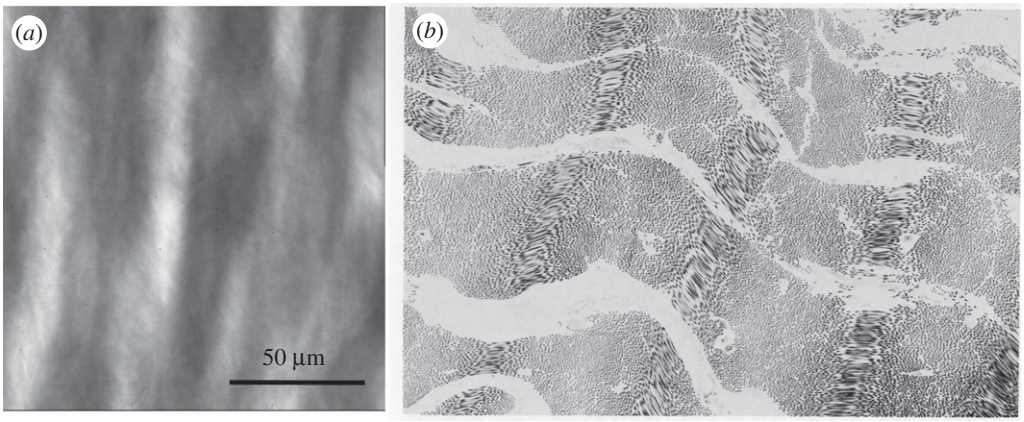

Figure 1. (*a*) Photomicrograph of native bovine pericardium showing the undulated collagen fibres (adapted from [8]). (*b*) TEM image also of native bovine pericardium clearly showing interrelationships between the undulated collagen fibres and the underlying fibril structures (magnification 4150×; adapted from [13]).

mechanical behaviour. Moreover, integration of such information into truly predictive modelling cannot proceed without accurate constitutive models of the EXL tissues and the subsequent fatigue processes [8,9].

The most common medical applications of cross-linked biologically-derived tissues are for dense collagenous tissues. Such tissues are typically composed of a dense, highly-organized network of type I collagen fibres, along with elastin, proteoglycans, glycosaminoglycans, cellular materials and a small amount of other fibrillar proteins. Type I collagen is the major determinant of its mechanical behaviour [10,11] and is the major tissue component affected by EXLs. At the molecular level, tropocollagen molecules are composed of a triple helix of three alpha chains [10,11] that arrange themselves into a quarter stacking array to form the collagen fibril [10,11]. Collagen fibrils form the functional subunits of the collagen fibres, as described by the Hodge–Petruska model [10,12], and then exhibit distinct large-scale structures (figure 1). Like the fibrils from which their functional properties are derived, collagen fibres exhibit high tensile but low flexural stiffness [14]. We note that there is no standard definition for a fibre and its relation to the fibril. They are very dependent on the specific tissues involved, and thus caution should always be exercised in the terminology used. In the mainstream tissue biomechanics literature, the fibre/fibril definition is often taken from the well-known work of Kastelic *et al*. [13], which focused on tendon. The pericardial tissues considered in this study clearly show fibre and fibril structures, including the fibre undulations commonly observed optically [15] (figure 1).

The fibre longitudinal/axial direction is the primary determinant of the stiffness of the tissue composite. Interestingly, collagen fibres typically have a stiffness of 1 GPa [15–18] and extend by no more than 4–5%. To increase the tissue-level compliance, collagen fibres at the macroscopic scale are sinusoidally crimped [10]. Tissue-level stress will not occur until the fibre-level crimp has been straightened. Moreover, the distribution of fibre straightening strains is the mechanism of tissue nonlinearity at large strains [19,20]. Thus, as in many other fields, the connection to the underlying structure can greatly inform our understanding of how collagenous tissues work and guide the development of mathematical models of their mechanical function.

While there is a wide range of application-specific chemical agents (e.g. riboflavin/UVA cross-linking for corneas), for mechanically-demanding and blood-contacting applications (e.g. BHVs) using collagenous tissues, an aqueous solution of glutaraldehyde (GLUT) is used. GLUT application is necessary to both biochemically and mechanically stabilize the tissue for *in vivo* use. During the cross-linking process GLUT rapidly permeates the tissue, with the cross-linking process largely complete within an hour and essentially stabilized by 24 h. Much of what we know about how GLUT EXLs alter the structures of collagenous tissues was reported by Nimni, Cheung and co-workers [21–27]. Briefly, GLUT reacts primarily with e-amino groups of lysyl residues in proteins, with Michael-addition reaction products of Schiff bases usually the final stable products. Based on the spectral characteristics and the molecular weights of the reaction products, it has been predicted that GLUT reacts with free amines to form an intermediate with a molecular weight of about 200 Da. The GLUT–polymer amine complex is self-limiting in size and can undergo internal rearrangement to become chemically inert. An increased molecular length of GLUT polymers from the initial glutaraldehyde and lysyl-residue reaction is more likely than an increased number of cross-linked sites. Following free GLUT depletion by binding to reactive groups, additional GLUT molecules attached to already reacted molecules can give rise to larger GLUT polymers that are able to generate 'long-range cross-links' between further removed reactive sites (figure 2). It is apparent from a mechanical behaviour perspective that GLUT-associated chemical cross-linking of the collagen structure and biochemistry can produce complex changes from the native state at the molecular, fibril, fibre and tissue levels.

To enable improved application of the use of EXL tissues in *in situ* treatment and prosthesis design, the development of physically realistic constitutive models is clearly required. In a previous work, a structural approach was used that incorporated experimentally measured angular distribution of collagen fibres and an assumed isotropic form for the EXL matrix [28]. Good agreement with the experimental data was observed, supporting the basic approach. An important utility of that early model was its ability to separate the effects of the fibres and matrix. However, it was only a first step; other factors such as bending rigidity of EXL fibres, fibre–fibre interactions, and fibre–matrix interactions were not considered. Moreover, the experimental data were reduced under the assumption of an isotropic Fung model; no rigorous investigation of the most appropriate form was undertaken.

The focus of the present work is to more fully investigate the underlying characteristics of the effects of EXLs on soft collagenous tissues, and to use this information to develop a

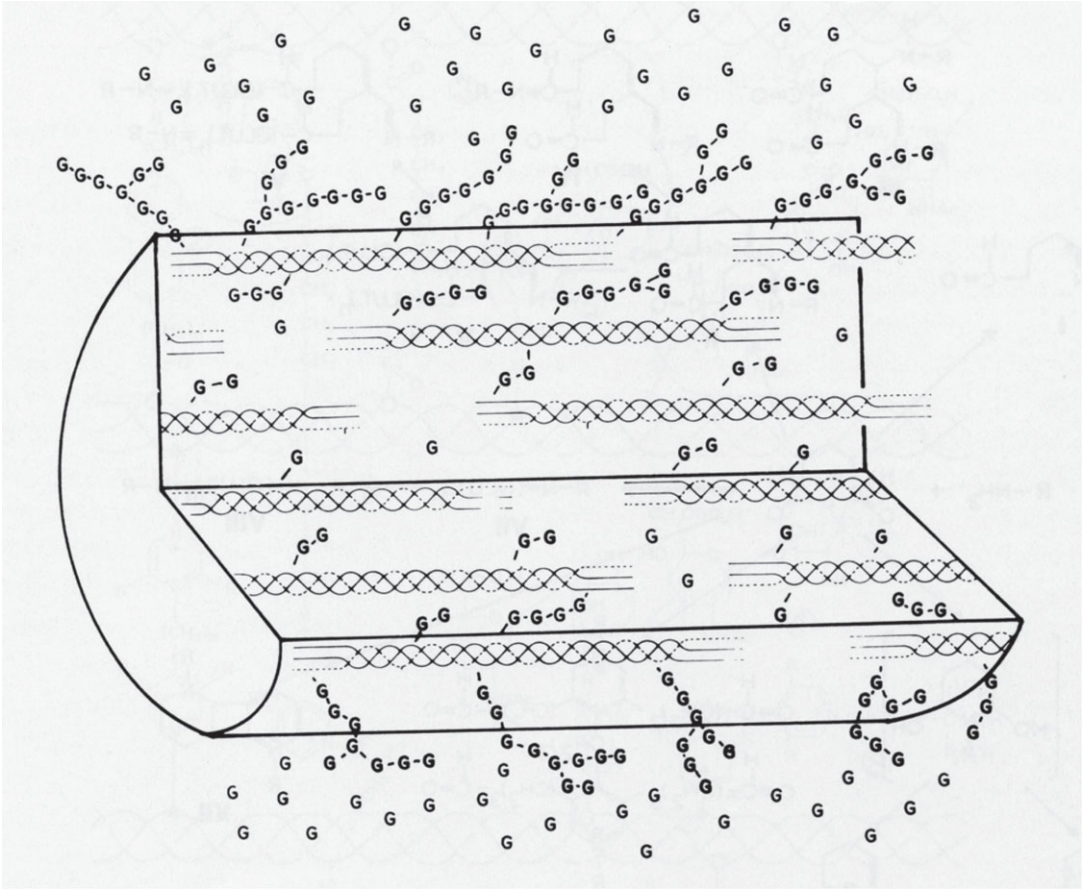

Figure 2. A diagram showing the interaction of tropocollagen molecules with glutaraldehyde and how cross-links can form. As the concentration of GLUT increases, the number of activation sites and chain length increases, and a limited number of cross-links will form between such molecules (magnification 4150×; adapted from [13]).

meso-scale (i.e. at the level of the fibre) structural constitutive model. In particular, we explored the following questions of the effects of EXLs on native collagenous tissues: (i) what are the effects on individual collagen fibres, (ii) what are the effects on single collagen fibre ensembles, (iii) are there interactions between fibre ensembles, and (iv) what is the functional form of the effective matrix response? This was done by exploiting experimental data from [29], wherein structurally controlled pericardial specimens were tested in the native state and then the EXL state. From these results, a comprehensive structural constitutive model was developed for EXL collagenous tissues and its predictive capability was evaluated. We note that, while we ultimately seek the micro-mechanical basis for macro-scale function, the present work is focused on a fibre-ensemble level approach.

2. Experimental methods and data post-processing

2.1. Tissue sources and experimental methods

Details of the tissue source, preparation and mechanical evaluation have been previously presented [29]. Briefly, large sections of native bovine pericardium were stored in phosphate-buffered saline (pH 7.4) at 4°C, then optically cleared using a hyperosmotic solution and the collagen fibre architecture (CFA) quantified. From the resulting CFA information, 25 × 25 mm test specimens exhibiting a high degree of structural uniformity suitable for biaxial testing were selected. The collagen fibre preferred and cross-preferred directions were aligned to the X_1–X_2 axes (figure 3). A total of five specimens were prepared in the native state.

Biaxial mechanical testing methods have been previously described in detail [30,31]. Briefly, testing was performed with the specimen immersed in phosphate-buffered normal saline (pH 7.4) at room temperature. First the Piola–Kirchhoff stress **P** controlled test protocol was used, wherein the ratio of the normal stress components $P_{11} : P_{22}$ was kept constant, with $P_{12} = P_{21} = 0$ and a maximum stress level of 1 MPa was used. Tissue deformations were quantified from the motion of four markers placed in the central third of the specimen, from which the deformation gradient tensor **F** was determined. For the first testing phase, an equi-biaxial stress protocol (i.e. $P_{11} : P_{22} = 1 : 1$) was used for both preconditioning and data acquisition. A total of 15 contiguous cycles were run with an approximate strain rate of $0.01\ s^{-1}$. Next, seven successive protocols were performed using ratios $P_{11} : P_{22} = 1 : 0.1$, $1 : 0.5$, $1 : 0.75$, $1 : 1$, $0.75 : 1$, $0.5 : 1$ and $0.1 : 1$. This range was chosen for extensive coverage of in-plane strain state. After testing, each native specimen was allowed to mechanically re-equilibrate by storing them in a stress-free state at 4°C for 24 h. Next, each specimen was chemically treated with 0.625% GLUT for a minimum of 72 h, with the tissue marker dimensions monitored throughout the cross-linking procedure, and then stored in phosphate-buffered normal saline at 4°C. As a final step, the above biaxial testing sequence was repeated. Data post-processing included

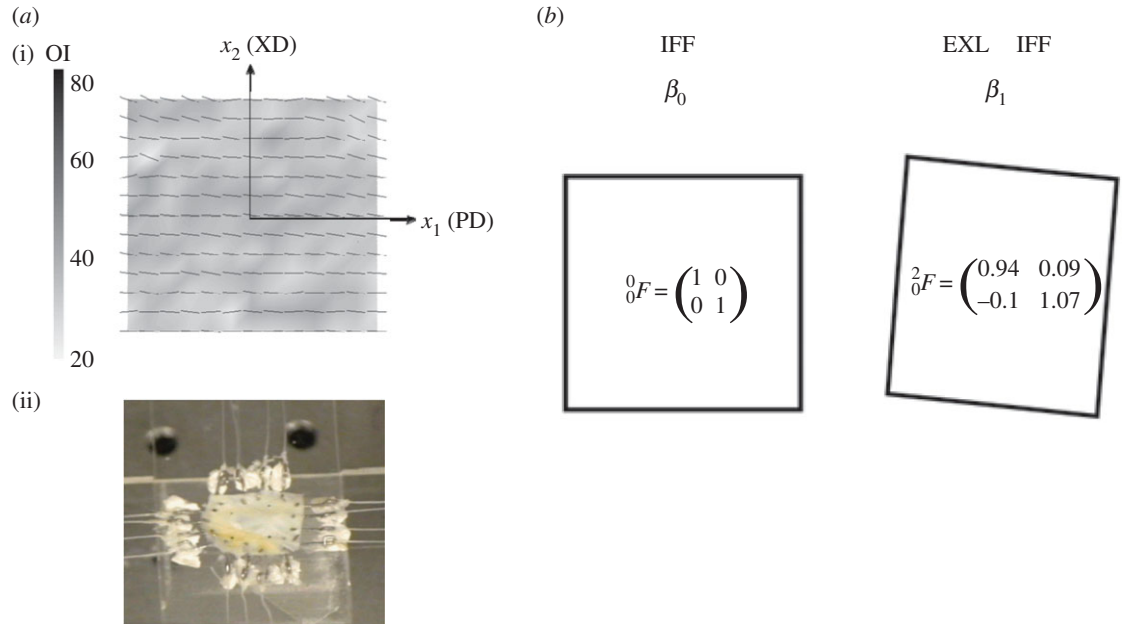

Figure 3. (*a*)(i) Pericardial test specimen showing a high degree of fibre orientation and uniformity in preferred fibre directions, with the PD $= x_1$ and XD $= x_2$ axes defined, and (ii) a typical biaxial test specimen mounted on the device. (*b*) A schematic of the biaxial test specimen geometry changes with cross-linking and the corresponding mean deformation gradient tensor components in native state β_0 and EXL state state β_1. Here, cross-linking induced a 6% contraction in the PD and and 7% direction in the XD, with some small shearing.

computation of the second Piola-Kirchhof tensor **S** and deformation gradient tensor **F** using established methods [32]. This test design allowed a comprehensive planar mechanical behaviour dataset to be collected on matched native and EXL specimens, compensating for inter-specimen variations.

2.2. Kinematic considerations and mechanical data post-processing

As observed in our other studies [29,32], the chemical fixation process will affect the specimen dimensions, and any analysis must carefully account for these effects on the collagen fibre kinematics. We thus defined the following configurations: β_0-native, β_1-EXL (figure 3*b*), used as the referential configurations for the native and EXL states, respectively. We represented all deformations using the notation for the deformation gradient tensor ${}^j_i\mathbf{F}$, where i and j represent the initial and final configurations, respectively (table 1). Values for the components of ${}^j_i\mathbf{F}$ were determined using the same method from §2.1 for the displacements of the four markers pre- and post-cross-linking for each specimen. Next, as first described by Lanir [19], we defined a fibre ensemble as a group of fibres with a common orientation. It has been shown that the ensemble stress–strain relation can be obtained from the interpolated equi-biaxial strain path, where $\mathbf{F} = \mathrm{diag}[\lambda, \lambda, 1/\lambda^2]$ using $S_c^{ens} = S_{11} + S_{22}$ [8]. To derive the equi-biaxial strain path ($\lambda_1 = \lambda_2$) from the stress-controlled experimental data, all mechanical data were combined and interpolated using cubic Hermite patches [33]. A strain path with $\lambda_1 = \lambda_2$ was interpolated within the range of the data as defined by the convex hull of $\{\lambda_1, \lambda_2\}$, and was implemented separately for each stress component (figure 4). To reliably overcome regions of sparse data we enforced the surface to be strictly convex everywhere. Finally, since the S_{12} component was negligible in all specimens, it was ignored in the subsequent analyses.

2.3. Establishing and modelling the mechanical behaviour of the native collagen fibre ensemble

Based on our previous tissue model findings [8,33–35], the dominant cause of the nonlinearity of the tissue-level mechanical behaviour of collagenous tissues is the gradual recruitment of collagen fibres [19]. The collagen fibres themselves behave linearly under typical fibre strains experienced under physiological stresses in tissues (2–5%). Once all fibres are fully straightened, the summed response should appear linear in the ensemble response. When applied to the equi-biaxial strain derived fibre-ensemble data, the upper bound can be directly determined as the transition point between the nonlinear and linear regions, with the slope of the linear region establishing the maximum tangent modulus (MTM) of the collagen fibre ensemble (e.g. [33]). The matrix response can also be determined from the pre-recruitment region where no collagen fibre have contributed. To determine the recruitment upper bound in the native tissue, we started at the largest measured strain and decreased the strain level until the region above was no longer linear. Linearity was defined from the mean squared error (MSE) of the linear regression to be less than 0.005% of the total MSE of all data, where $\mathrm{MSE} = \sum_i^n (S^i_{ens} - \bar{S}_{ens})/n$. Similarly, we determined the lower bound by starting at zero strain and increasing the strain until a deviation from linearity was determined.

Next, we note that in some previous structural models a fibre stress–strain relation linear in the second Piola-Kirchhoff stress and Green Lagrange strain has been used [8,34,36]. However, SAXS studies have demonstrated a linear force–displacement relation for collagen fibrils in the tendon [37,38] and MV tissue [39,40]. This is further corroborated by the atomistic modelling results by Buehler [41], where the force–displacement relation is essentially linear at strains lower than 0.35. We have recently determined that for the mitral valve leaflet the tissue level-derived collagen fibre mechanical behaviour is actually quite linear, with an effective modulus of

Table 1. Nomenclature.

int	interaction term
c	collagen
m	matrix
EB	equibiaxial
ODF	orientation distribution function
$\mathbf{F}$	deformation gradient tensor
$\mathbf{E}$	Green Lagrange strain tensor
$\mathbf{P}$	first Piola Kirchhoff stress tensor
$\mathbf{S}$	second Piola Kirchhoff stress tensor
$\mathbf{C}$	right Cauchy Green strain tensor
$\mathbf{n_0}$, $\mathbf{m_0}$	fibre-ensemble orientation vectors
ens	ensemble
λ	stretch
λ_s	slack stretch
λ_t	true fibre stretch
E_s	slack strain
Ψ	strain energy
ϕ	mass fraction
D	distribution of slack strains for fibre recruitment
Γ	fibre ODF
η	modulus, subscript for elastin collagen and matrix
μ_θ	mean circumferential orientation
σ	standard deviation of the fibre splay
μ_r	mean of the recruitment distribution
σ_r	standard deviation of the recruitment distribution
λ_{lb}	lower bound of the recruitment distribution
λ_{ub}	upper bound of the recruitment distribution
c_0, c_1,	exponent for intra-fibre-ensemble interaction terms
d_0, d_1	exponent for inter-fibre-ensemble interaction terms

approximately 160 MPa. Based on these considerations, we assumed for the native collagen fibres that

(1) they exhibit a linear P–λ response
(2) slack stretch of the collagen fibres does not vary with orientation.

From these two basic considerations, we used the following effective native collagen fibre model [33,34]. We start by defining the native collagen fibre strain energy as

$$\Psi_f(\lambda_t) = \begin{cases} \frac{\eta_c}{2}(\lambda_t - 1)^2 & \text{for } \lambda_t \geq 1 \\ 0 & \text{for } \lambda_t < 1, \end{cases} \tag{2.1}$$

where $\lambda_t = \lambda_f/\lambda_s$ is the true stretch of the fibre. This leads to the following P–λ form using $P_f = \partial\Psi(\lambda_f)/\partial\lambda_f = \partial\Psi(\lambda_t)/\partial\lambda_t \cdot \partial\lambda_t/\partial\lambda_f$

$$P_f = \begin{cases} \frac{\eta_c}{\lambda_s}(\lambda_t - 1) & \text{for } \lambda_t \geq 1 \\ 0 & \text{for } \lambda_t < 1, \end{cases} \tag{2.2}$$

where P_f is the first Piola-Kirchhoff stress of the fibre, η_c is the modulus of the fibre, λ_f is the fibre stretch and λ_s is the fibre slack stretch. Next, we use this fibre model in the expression for the native collagen fibre ensemble using

$$\left.\begin{aligned} P_c^{ens} &= \phi_c \eta_c \int_1^{\lambda_\theta} \frac{D(x)}{x}\left(\frac{\lambda_\theta}{x} - 1\right)dx \\ \text{and} \quad \frac{\partial P_c^{ens}}{\partial \lambda_\theta} &= TM_c^{ens} = \phi_c \eta_c \int_1^{\lambda_\theta} \frac{D(x)}{x^2}dx, \end{aligned}\right\} \tag{2.3}$$

where ϕ_c is the collagen fibre mass fraction, λ_θ is the fibre-ensemble stretch along the direction defined by θ (computed from the tissue-level deformation using $\lambda_\theta = \mathbf{F} \cdot \mathbf{n}(\theta)$), and $D(\lambda_s)$ is the probability distribution function describing the distribution of collagen fibre slack length within the ensemble. We assumed $D(\lambda_s)$ is Beta distributed, so that

$$\left.\begin{aligned} D(\alpha, \beta, \lambda_{ub}, \lambda_{lb}, \lambda_s) &= \begin{cases} \frac{y^{\alpha-1}(1-y)^{\beta-1}}{B(\alpha,\beta)(\lambda_{ub}-\lambda_{lb})} & \text{for } y \in [0,1] \\ 0, & \text{otherwise,} \end{cases} \\ y &= \frac{\lambda_s - \lambda_{lb}}{\lambda_{ub} - \lambda_{lb}}, \quad \bar{\mu} = \frac{\mu - \lambda_{lb}}{\lambda_{ub} - \lambda_{lb}} \\ \text{and} \quad \bar{\sigma} &= \frac{\sigma}{\lambda_{ub} - \lambda_{lb}}, \quad \alpha = \frac{\bar{\mu}^2 - \bar{\mu}^3 - \bar{\sigma}^2\bar{\mu}}{\bar{\sigma}^2}, \\ \beta &= \alpha\frac{1-\bar{\mu}}{\bar{\mu}}, \end{aligned}\right\} \tag{2.4}$$

where λ_{lb} and λ_{ub} are the lower and upper bound stretch of the collagen fibre recruitment, respectively. Note that in preliminary examinations of the data we found that all specimens exhibited distinct pre- and post-transition locations (figure 5), allowing λ_{lb}, λ_{ub} to be determined directly from the collagen fibre ensemble data. Thus, the complete initial ensemble model (equation (2.3)) has three parameters (η_c, α, β) to fit to the data using standard techniques [33].

3. Delineation and modelling of the tissue-level mechanical effects of exogenous cross-links

3.1. Rationale

While extensive work has been done on the characterization of the biomechanical effects of EXL formation on soft tissues [29,42–54], there has been surprisingly little work done known to the authors on the development of formal constitutive models (other than [28]). Related work on proteoglycan and related collagen fibril sub-forms have revealed complex micromechanical interactions (e.g. [55,56]), but micromechanical interactions modified by EXLs on the macroscale tissue responses remain largely unknown. Thus, prior to developing the constitutive model form, we first carefully examined the effects of EXL formation on the measured tissue-level biomechanical behaviours in the present dataset.

3.2. Effects of exogenous cross-link formation on collagen fibre ensembles

All specimens exhibited anisotropic dimensional changes due to preconditioning and cross-linking (figure 3*b*). Interestingly, we found that about 6% shrinkage occurred in the preferred direction, and approximately 7% expansion in the cross-preferred directions. Such changes can alter both the angular dependence on collagen recruitment and the

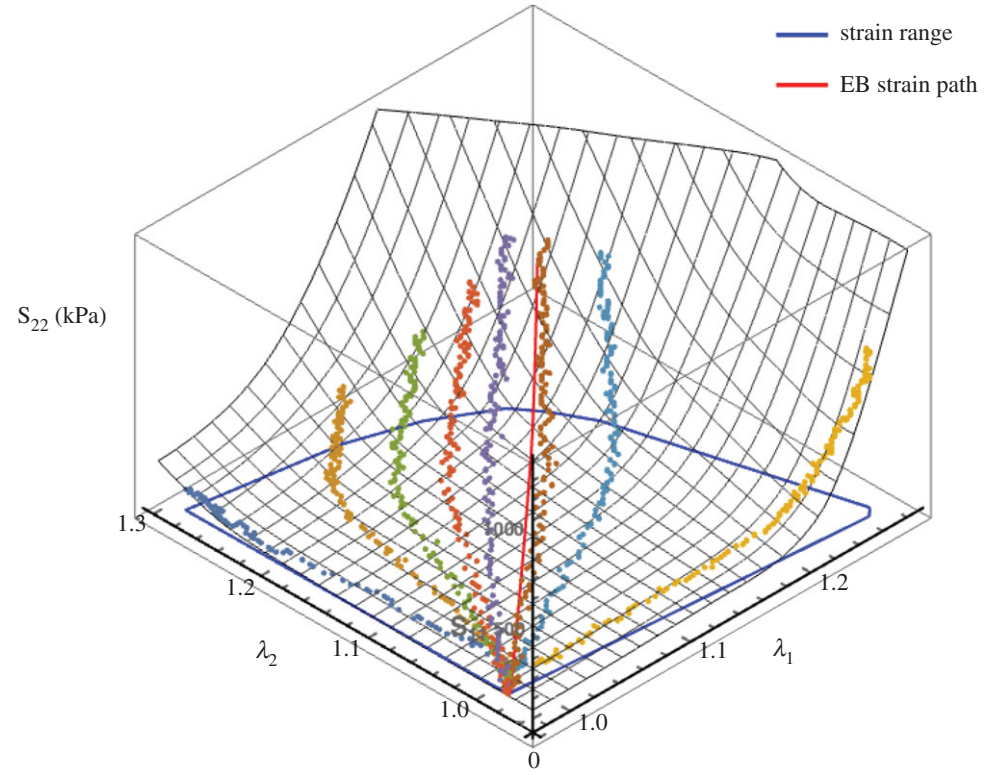

Figure 4. An example of the bicubic Hermite surface interpolation of the S_{22} biaxial test responses to allow interpolation of an equi-biaxial strain path, shown here in red. The blue path defines the span of the strain.

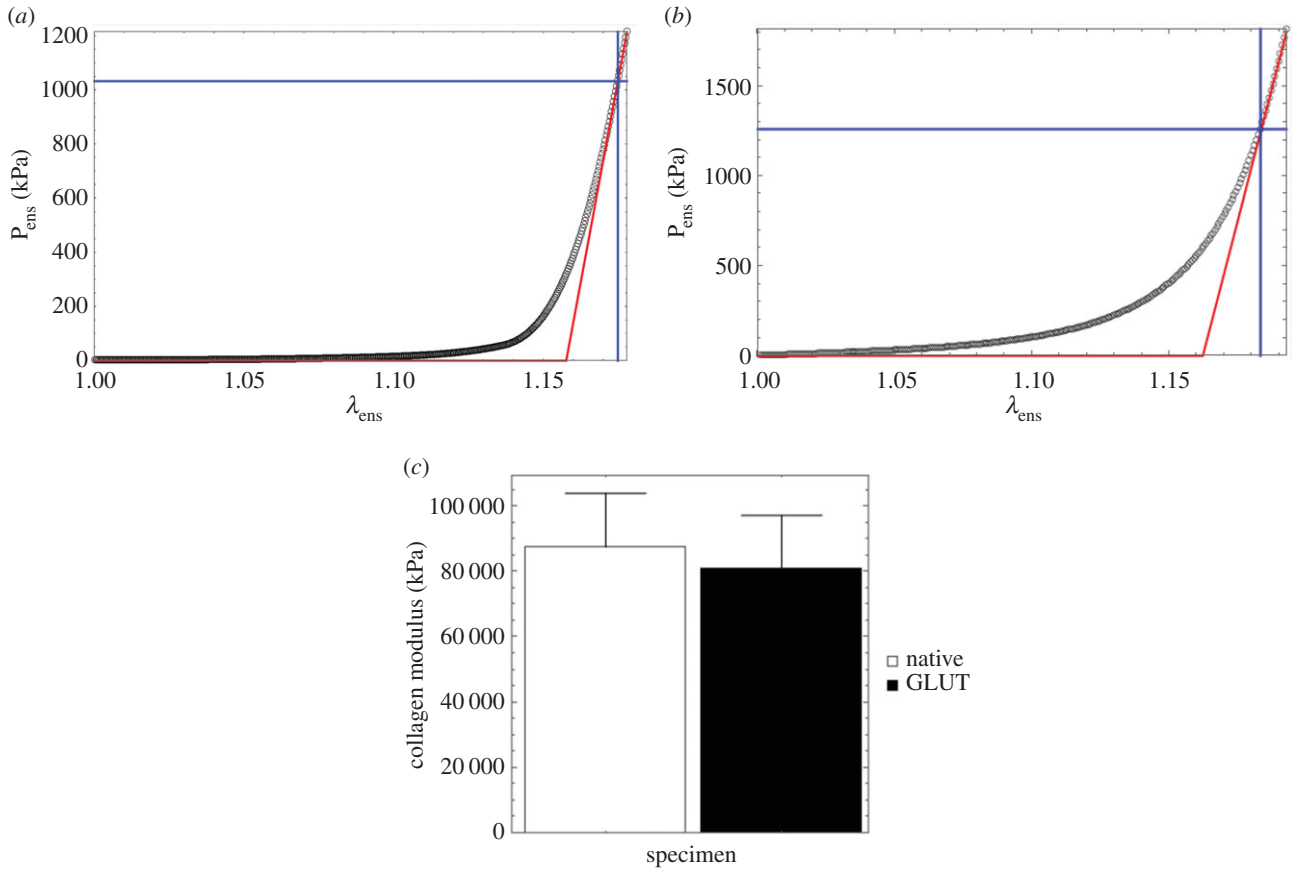

Figure 5. A representative fibre-ensemble stress–strain (in $P_{ens} - \lambda_{ens}$) response for (*a*) native and (*b*) cross-linked bovine pericardium illustrating a well-defined post-transition fibre recruitment point wherein the response becomes linear. While the native pericardium demonstrated a very low initial modulus (approx. 75 kPa; table 2), the EXLs demonstrate a significantly stiffer modulus. (Online version in colour.)

collagen fibre orientation distribution. We determined basic characteristics of the collagen fibre stress–strain relations directly from the data (no modelling), including the lower and upper bound-associated stresses, the initial tangent modulus, and the MTM from a running 15-point window. From this analysis, we were able to determine a number of

Table 2. Key collagen fibre-ensemble results for the native and matched GLUT EXL specimens, both reference to β_1.

ID	12	21	41	61	68	mean	s.e.m.	*p*-value
initial tangent modulus (kPa)								
native	73.9	65.6	25.5	110.63	107.3	76.6	17.4	
GLUT	1059.3	248.4	152.4	746.0	272.1	495.6	195.2	0.037
MTM (kPa)								
native	54 208.09	49 014.0	53 091.2	72 459.7	77 121.2	61 179.0	6341.28	
GLUT	67 771.3	28 614.8	58 025.2	62 319.2	70 717.5	57 489.6	8433.78	0.566726
upper bound stress (kPa)								
native	1164.05	885.392	956.206	1048.43	1289.37	1068.69	80.7988	
GLUT	1081.74	925.842	1204.19	1138.22	1353.78	1140.75	78.6925	0.245422

important mechanical characteristics (table 2 and figure 5). These include:

(1) All specimens exhibited an approximately 6.5-fold increase in the initial tangent modulus (table 2), very similar to values and native/EXL ratios reported in [54], which were conducted under flex conditions.
(2) The upper bound stress and MTM were found to be unaffected by EXL formation (table 2).
(3) EXL formation induced a reduction in achieved strain levels compared with the native state (figure 5*a*).
(4) The effective collagen modulus was unaffected by EXL formation (figure 5*c*).

Collectively, these results reveal some important features of the effects of EXLs on collagen tissues. First, as noted in our previous studies [28,54] EXLs produce a substantial increase in the low-strain modulus. Next, equation (2.3) indicates that the MTM is proportional to the collagen fibre modulus and the recruitment function D. Use of equation (2.3) compensates for the effect of the changes in tissue dimensions due to cross-linking on the fibre recruitment, allowing separation of changes in fibre architecture from the modulus on the ensemble stress–strain curve. Thus, the lack of changes in effective modulus are independent of any effects of changes resulting from tissue dimensions and represent an accurate modulus estimate.

4. Initial model formulation

4.1. General approach

The above findings provide sufficient information to develop a new model. In the present study, we assume EXLs induce fibre–fibre and fibre–matrix interactions that are mechanically significant. We ignore any time-dependent effects, as we have found that native and cross-linked valvular tissues exhibit minimal time-dependent effects [57–60]. Next, we assume that the pericardial tissues considered are only composed of collagen fibres and a matrix constituent that represents non-cross-linked and cross-linked components, and water. The contributions from elastin or other tissue components are ignored, because they have either negligible mass or stiffness. In all previous structural models of soft tissues, interactions between components (fibres, matrix) have been ignored. As we cannot assume this in the present investigation, we use the following hyperelastic general form:

$$\Psi(\mathbf{C}) = \phi_c[\Psi_c(\mathbf{C}) + \Psi_{int}(\mathbf{C})] + (1-\phi_c)\Psi_m(\mathbf{C}) + p(J-1), \tag{4.1}$$

where ϕ_c is the mass fraction of the collagen fibres, Ψ_c, Ψ_m and Ψ_{int} are the strain energy density functions of the collagen, matrix and interaction terms, respectively, $J = \det(\mathbf{F})$, and p is the Lagrange multiplier to enforce incompressibility. The resulting tissue-level response in terms of the second Piola-Kirchhoff stress tensor $\mathbf{S}$ is given by

$$\begin{aligned}\mathbf{S} &= 2\frac{\partial \Psi}{\partial \mathbf{C}} - p\mathbf{C}^{-1} \\ &= 2\left[\phi_c \frac{\partial \Psi_c}{\partial \mathbf{C}} + (1-\phi_c)\frac{\partial \Psi_m}{\partial \mathbf{C}} + \phi_c \frac{\partial \Psi_{int}}{\partial \mathbf{C}}\right] - p\mathbf{C}^{-1}.\end{aligned} \tag{4.2}$$

4.2. Accounting for changes in tissue dimensions for the collagen phase

Results from §3 suggest that the native collagen fibre modulus is unaffected by cross-linking. However, the observed changes in tissue dimensions can also induce changes in tissue-level mechanical behaviour by altering the structure due to tissue shrinkage. This essentially results in a different reference configuration. There is thus a need to reformulate structural models to account for these effects directly. The formulation described in the following allows handling of changes in tissue reference state geometry. The key assumptions are:

(1) Changes are due to alterations in the initial geometric configuration only, so that
   (a) Mass fractions of each phase remain unchanged.
   (b) The internal mechanical energy remains zero. Thus, all changes in internal component configurations are not associated with any change in internal energy (which remains zero)—just initial configuration (e.g. fibre orientation, degree of undulation, thickness and length).
(2) Tissue dimensions and internal architecture change under the *affine* kinematic assumption. Thus, the configuration of all constituent fibres in the altered reference state (after all changes in initial specimen

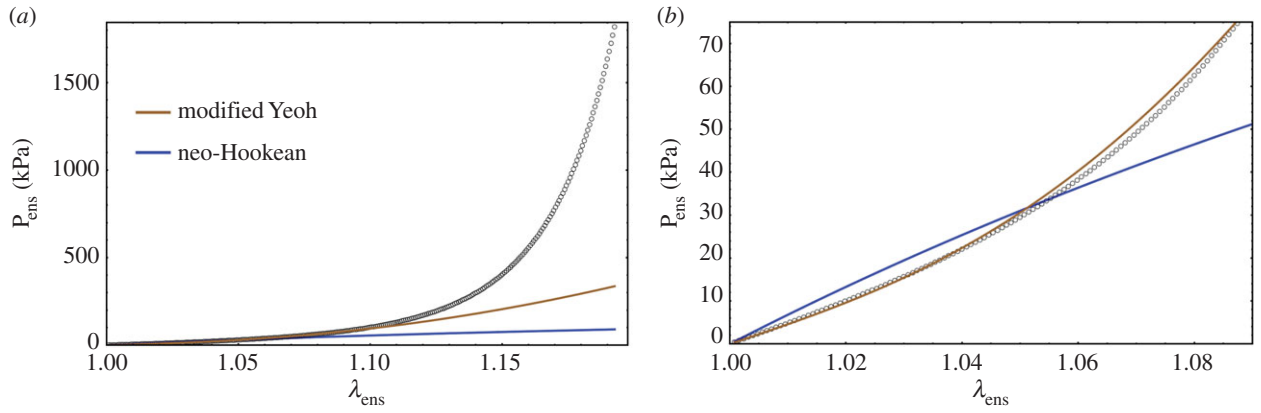

Figure 6. (*a*) A representative fibre-ensemble stress–strain (in $P_{ens}-\lambda_{ens}$) response for EXL treated bovine periardium, and (*b*) a close-up of the low stress region. A careful examination revealed that the toe region suggests that a modified Yeoh model was necessary to accurately capture its response (equation (4.8)) due to the convexity of the response. (Online version in colour.)

geometry have taken place) can be predicted. Moreover, the configurational change is homogeneous, and can be thus described by a deformation gradient tensor with constant components.

(3) To be consistent with the fibre recruitment mechanisms (e.g. [8,33]), all fibres remain undulated in the new reference state.

(4) The matrix phase is unaffected by the geometric configuration changes and is referenced to β_1 (figure 3*b*) for all subsequent stress calculations.

As a first step, we recast the recruitment function parameters determined in β_0 but mapped to β_1 using

$$\left.\begin{aligned} &D_1(\mu_0,\,\sigma_0,\,{}_0\lambda_{\rm lb},{}_0\lambda_{\rm ub},\,{}^1_0\lambda,\,{}_1\lambda_s)\\ &\quad=\begin{cases}\dfrac{y^{\alpha-1}(1-y)^{\beta-1}}{B(\alpha,\,\beta)({}_1\lambda_{\rm ub}-{}_1\lambda_{\rm lb})} & y\in[0,\,1]\\ 0 & \text{otherwise}\end{cases}\\ &y=\frac{{}^t_1\lambda_s-{}_1\lambda_{\rm lb}}{{}_1\lambda_{\rm ub}-{}_1\lambda_{\rm lb}},\quad {}_1\lambda_{\rm lb}=\frac{{}_0\lambda_{\rm lb}}{{}^1_0\lambda},\quad {}_1\lambda_{\rm ub}=\frac{{}_0\lambda_{\rm ub}}{{}^1_0\lambda}\\ &\bar\mu=\frac{\mu_0-{}_0\lambda_{\rm lb}}{{}_0\lambda_{\rm ub}-{}_0\lambda_{\rm lb}},\quad \bar\sigma=\frac{\sigma_0}{{}_0\lambda_{\rm ub}-{}_0\lambda_{\rm lb}}\\ \text{and}\quad &\alpha=\frac{\bar\mu^2-\bar\mu^3-\bar\sigma^2\bar\mu}{\bar\sigma^2},\quad \beta=\alpha\frac{1-\bar\mu}{\bar\mu},\end{aligned}\right\}\tag{4.3}$$

where the left subscript denotes the configuration state. Note carefully that ${}^1_0\lambda$ will in general be a function of θ_1, so that even though the collagen fibre recruitment is orientation-independent in β_0, it will have angular dependence in β_1 unless ${}^1_0F_{11}={}^1_0F_{22}$, ${}^1_0F_{12}={}^1_0F_{21}=0$. The resulting expression for the ensemble stress is

$${}^t_1S^{\rm ens}_c=\frac{\phi_c\eta_c}{{}^t_1\lambda}\int_1^{{}^t_1\lambda}\frac{D_1(\mu_0,\,\sigma_0,\,{}_0\lambda_{\rm lb},\,{}_0\lambda_{\rm ub},\,{}^1_0\lambda,\,x)}{x}\left(\frac{{}^t_1\lambda}{x}-1\right)\mathrm{d}x.\tag{4.4}$$

To complete the tissue-level formulation, we use the affine transformation assumption and the formulation described in [34] to obtain the collagen fibre orientation distribution function Γ_0 in the native state to that in β_1 using

$$\Gamma_1[\mu_\Gamma,\,\sigma_\Gamma,\,\theta_1]=\Gamma_0\left[\mu_\Gamma,\,\sigma_\Gamma,\,\theta_0({}^1_0\mathbf{F},\,\theta_1)\right]\frac{{}^1_0\lambda^2_{\theta_0}}{{}^1_0J_{2D}}.\tag{4.5}$$

Note that the angle θ_1 of a fibre originally oriented at θ_0 can be determined using

$$\theta_1({}^1_0\mathbf{F},\,\theta_0)=\tan^{-1}\left(\frac{{}^1_0F_{12}\cos(\theta_0)+{}^1_0F_{22}\sin(\theta_0)}{{}^1_0F_{11}\cos(\theta_0)+{}^1_0F_{12}\sin(\theta_0)}\right).\tag{4.6}$$

The final form of the native collagen fibre phase expressed in the EXL state is thus

$${}^t_1\mathbf{S}_c(\eta_c,\mu_\Gamma,\sigma_\Gamma,\mu_0,\sigma_0)=\frac{\phi_c\eta_c}{{}^t_1\lambda}\int_{\theta_1}\Gamma_1[\mu_\Gamma,\sigma_\Gamma,\theta_1]\times\left\{\int_1^{{}^t_1\lambda}\frac{D_1(\mu_0,\sigma_0,{}_0\lambda_{\rm lb},{}_0\lambda_{\rm ub},{}^1_0\lambda[\theta_0(\theta_1)],x)}{x}\left(\frac{{}^t_1\lambda}{x}-1\right)\mathrm{d}x\right\}\mathbf{n}_1\otimes\mathbf{n}_1\,\mathrm{d}\theta_1.\tag{4.7}$$

The above equation has a total of five fitted model parameters η_c, μ_m, μ_Γ, σ_Γ, $\sigma 0$ ($\lambda_{\rm lb}$, ${}_0\lambda_{\rm ub}$ are determined from the experimental data), all with a physical meaning and all referred to β_0.

4.3. The matrix phase

The matrix response can be estimated from the low stress region where collagen does not contribute any stress (figures 5 and 6). A careful examination revealed that the toe region is a convex curve in S–λ, which is inconsistent with a neo-Hookean material model which is concave in S–λ (figure 6). While we have used an exponential isotropic function for the matrix before [28], we considered the Yeoh model but found it unable to fit the data. Therefore, we developed a modified Yeoh model as

$$\left.\begin{aligned}&\Psi_m(\mathbf{C})=\frac{\mu_a}{2\alpha}(I_1-3)^a+\frac{\mu_b}{2b}(I_1-3)^b\\ \text{and}\quad &\mathbf{S}_m=(\mu_a(I_1-3)^{b-1}+\mu_b(I_1-3)^{b-1})(\mathbf{I}-C_{33}\mathbf{C}^{-1}),\\ &\qquad\text{with } 1<a<b,\quad a\cdot b<2.\end{aligned}\right\}\tag{4.8}$$

When applied to all pre-transition mechanical data (i.e. from all protocols and where there is no collagen fibre contribution), this form was found to fit the low-stress data quite well (figure 6).

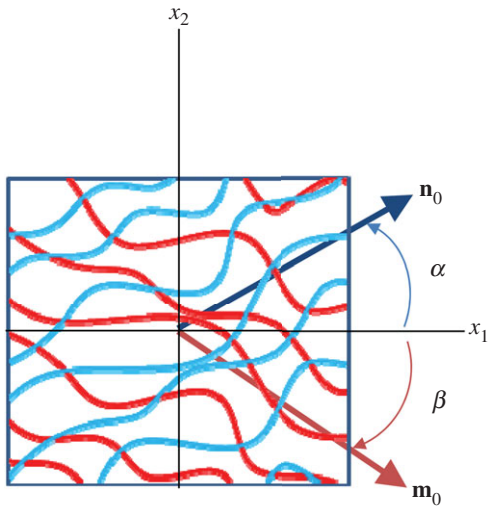

Figure 7. A schematic of two collagen fibre ensembles with respective orientations α and β (not restricted to be symmetric about the x_1-axis) with associated orientation vector $\mathbf{n}_0$ and $\mathbf{m}_0$ in the reference configuration. (Online version in colour.)

4.4. Interactions

Our key working assumption is that all fibre–fibre and fibre–matrix interactions can be represented at the *fibre-ensemble level*. This is done to simplify the model formulation, and further since the exact micromechanical mechanisms of cross-linking have yet to be determined. Based on the form assumed in equation (4.2), we now have the ability to estimate the form and magnitude of the fibre-ensemble interactions from the fibre-ensemble data using $\mathbf{S}_{\text{int}} \approx \mathbf{S}_{\text{ens}} - 1/\varphi_c(\varphi_c\mathbf{S}_c + (1-\varphi_c)\mathbf{S}_m)$, where $\mathbf{S}_{\text{ens}}$ is the ensemble stress (figure 5). Note here that the collagen stress $\mathbf{S}_c = {}^t_1\mathbf{S}_c$, and is thus the contribution of the collagen fibres expressed in the EXL configuration β_1 using equation (4.7). This approach allowed us to exploit the matched native–EXL mechanical data by fitting the native responses then mapping them to the EXL state, so that they are a known quantity rather than one that required data fitting. Results of this analysis indicated some intriguing results. First, while the collagen phase contributed substantially to the total ensemble stress, it was only about 50%, and the matrix only about 20%. This revealed that the remaining approximately 30% portion of the total ensemble stress must be a result of the interaction mechanisms.

To model the interactions, we first consider two fibre ensembles with orientation vectors $\mathbf{n}_0(\alpha)$ and $\mathbf{m}_0(\beta)$ in the reference configuration (figure 7). These two ensembles can mechanically interact by elongation and relative rotation. Kinematically, these mechanisms can be captured using the pseudo-invariant I_8 [61,62]

$$\left.\begin{aligned} \mathrm{I}_8 &= \mathbf{n}_0 \cdot \mathbf{C}\mathbf{m}_0 = \cos(\theta)\,\lambda_\alpha\lambda_\beta \\ \cos(\theta) &= \frac{\mathbf{n}\cdot\mathbf{m}}{\lambda_\alpha}\lambda_\beta, \quad \lambda_\alpha = \sqrt{\mathbf{n}_0\cdot\mathbf{C}\mathbf{n}_0}, \quad \lambda_\beta = \sqrt{\mathbf{m}_0\cdot\mathbf{C}\mathbf{m}_0}. \end{aligned}\right\} \tag{4.9}$$

Note that we can also use $I_8' = I_8 - I_8^0$ [62] to account for the relative change in fibre rotations if necessary. Thus, I_8 can be considered the product of an extensional term $\lambda_\alpha\lambda_\beta$ and a rotational term $\cos(\theta)$. We consider two sub-aspects of ensemble-level effects: intra- and inter-ensemble levels. The intra-ensemble incorporates all fibre–fibre interactions that occur within a single ensemble and are limited to extensional effects only. By contrast, inter-ensemble effects can include both extensional and rotational effects.

To best capture these phenomena, we do not use I_8 directly but rather the following forms. The results for the ensemble stress suggest that the interaction terms are exponential in character (figure 8). Thus, for the extensional intra-ensemble effects we use

$$\Psi^e_{\text{int}}(\mathbf{C}) = \frac{c_0}{4}\int_\theta \Gamma(\theta)[e^{c_1(\lambda-1)^2} - 1]\,\mathrm{d}\theta, \tag{4.10}$$

where $\lambda = \sqrt{\mathbf{n}_0\cdot\mathbf{C}\mathbf{n}_0} = \sqrt{I_4}$ and c_0, c_1 are constants, and the associated single ensemble stress extensional interaction is

$$\begin{aligned} \mathbf{S}^e_{\text{int}} &= 2\frac{\partial\,\Psi(\mathbf{C})}{\partial\mathbf{C}} = 2\frac{\partial\,\Psi(\lambda)}{\partial\lambda}\cdot\frac{\partial\lambda}{\partial\mathbf{C}} \\ &= \int_\theta \Gamma(\theta)\left[\frac{c_0c_1(\lambda-1)\mathrm{e}^{c_1(\lambda-1)^2}}{\lambda}(\mathbf{n}_0\otimes\mathbf{n}_0)\right]\mathrm{d}\theta. \end{aligned} \tag{4.11}$$

Next, for the *extensional inter-ensemble* interactions, we use a similar form

$$\Psi^{ee}_{\text{int}}(\mathbf{C}) = \frac{d_0}{4}\int_\alpha\int_\beta \Gamma(\alpha)\Gamma(\beta)\left[\mathrm{e}^{d_1(\lambda_\alpha\lambda_\beta-1)^2} - 1\right]\mathrm{d}\alpha\,\mathrm{d}\beta, \tag{4.12}$$

where d_0 and d_1 are constants, with associated stresses

$$\begin{aligned} \mathbf{S}^{ee}_{\text{int}} = \int_\alpha\int_\beta \Gamma(\alpha)\Gamma(\beta)\Bigg[&d_0d_1(\lambda_\alpha\lambda_\beta-1)\mathrm{e}^{d_1(\lambda_\alpha\lambda_\beta-1)^2} \\ &\times\left[\frac{\lambda_\beta}{\lambda_\alpha}(\mathbf{n}_0\otimes\mathbf{n}_0) + \frac{\lambda_\alpha}{\lambda_\beta}(\mathbf{m}_0\otimes\mathbf{m}_0)\right]\Bigg]\mathrm{d}\alpha\,\mathrm{d}\beta. \end{aligned} \tag{4.13}$$

Note that the exponential term was set to zero if $\lambda_\alpha\lambda_\beta \le 1$. In this approach, we integrate over all ensembles, weighted by their respective orientation distribution functions, to obtain the total contribution.

Next, we developed a rotational pseudo-invariant defined as the change in the cosine between the two ensemble fibre directions, which is simply

$$I^r_{\text{int}}(\alpha,\beta) = \frac{I_8}{\lambda_\alpha\lambda_\beta} - \mathbf{n}_0\cdot\mathbf{m}_0 = \cos(\theta) - \cos(\theta_0) \approx \Delta\theta. \tag{4.14}$$

Using $\Psi^r_{\text{int}}(\mathbf{C}) = \frac{\eta^r}{4}(I^r_{\text{int}})^2$, it can be shown that for planar distributed fibre ensembles the stress tensor is

$$\begin{aligned} \mathbf{S}^r_{\text{int}} = \eta^r\int_\alpha\int_\beta \Gamma(\alpha)\Gamma(\beta)\frac{I^r_{\text{int}}(\alpha,\beta)}{\lambda_\alpha\lambda_\beta}\Bigg[&(\mathbf{m}_0\otimes\mathbf{n}_0 + \mathbf{n}_0\otimes\mathbf{m}_0) \\ &-I_8\left(\frac{\mathbf{n}_0\otimes\mathbf{n}_0}{\lambda_\alpha^2} + \frac{\mathbf{m}_0\otimes\mathbf{m}_0}{\lambda_\beta^2}\right)\Bigg]\mathrm{d}\alpha\,\mathrm{d}\beta. \end{aligned} \tag{4.15}$$

Combining equations (4.7), (4.8), (4.11), (4.13) and (4.15), we obtain the final form of the full model stress as

$$\begin{aligned} \mathbf{S} = {}&\phi_c\mathbf{S}_c(\eta_c,\mu_\Gamma,\sigma_\Gamma,\mu_0,\sigma_0) + (1-\phi_c)\mathbf{S}_m(a,b,\mu_a,\mu_b) \\ &+ \phi_c(\mathbf{S}^e_{\text{int}}(c_0,c_1) + \mathbf{S}^{ee}_{\text{int}}(d_0,d_1) + \mathbf{S}^r_{\text{int}}(\eta^r)) - p\mathbf{C}^{-1}. \end{aligned} \tag{4.16}$$

5. Model simplifications and parameter estimation

5.1. Final form

While in principle equation (4.16) can be implemented within a robust parameter estimation procedure, simplifications are

clearly in order given its complexity (14 parameters). We first consider an equi-biaxial test wherein all fibre rotations are zero, so that $I^{r}_{\text{int}} = 0$. The total interaction stress is thus given by just the following extensional contributions:

$$\begin{aligned}\mathbf{S}_{\text{int}} = &\int_{\theta} \Gamma(\theta)\left[\frac{c_0 c_1(\lambda-1)\mathrm{e}^{c_1(\lambda-1)^2}}{\lambda}(\mathbf{n}_0\otimes\mathbf{n}_0)\right]\mathrm{d}\theta \\ &+\int_{\alpha}\int_{\beta}\Gamma(\alpha)\Gamma(\beta)\Big[d_0 d_1(\lambda^2-1)\mathrm{e}^{d_1(\lambda^2-1)^2}\big[(\mathbf{n}_0\otimes\mathbf{n}_0) \\ &+(\mathbf{m}_0\otimes\mathbf{m}_0)\big]\Big]\mathrm{d}\alpha\,\mathrm{d}\beta.\end{aligned} \tag{5.1}$$

In practice, we found that while the intra-ensemble form (first r.h.s. term) was used alone it was able to capture the equi-biaxial strain behaviour (figure 5), it was unable to capture the response from all test protocols. Moreover, given the similarity in form, the two components on the r.h.s. of equation (5.1) can capture similar responses. We thus chose to ignore the intra-ensemble stress contribution $\mathbf{S}^{\text{e}}_{\text{int}}(c_0, c_1)$, removing two parameters. Next, while it is intuitive that fibre-ensemble rotations produce important contributions to the total tissue stress, closer analysis of equation (4.15) indicated that it will produce compressive stresses in the direction of lesser stretch. These characteristics were not consistent with any of the observed experimental data. Even when choosing various forms of $\Psi^{r}_{\text{int}}(\mathbf{C})$, we could not match the experimentally observed responses. Interestingly, only the $\mathbf{S}^{ee}_{\text{int}}(d_0, d_1)$ contribution of equation (4.16) was found to model the interaction stresses well.

Thus, we are left with the following interaction stresses:

$$\begin{aligned}\mathbf{S}_{\text{int}} = &\int_{\alpha}\int_{\beta}\Gamma(\alpha)\Gamma(\beta)\Big[d_0 d_1(\lambda_\alpha\lambda_\beta-1)\mathrm{e}^{d_1(\lambda_\alpha\lambda_\beta-1)^2} \\ &\times\left[\frac{\lambda_\beta}{\lambda_\alpha}(\mathbf{n}_0\otimes\mathbf{n}_0)+\frac{\lambda_\alpha}{\lambda_\beta}(\mathbf{m}_0\otimes\mathbf{m}_0)\right]\Big]\mathrm{d}\alpha\,\mathrm{d}\beta,\end{aligned} \tag{5.2}$$

leading to the following *final form* of the constitutive model:

$$\left.\begin{aligned}\mathbf{S} &= \mathbf{S}_{\text{c}}+\mathbf{S}_{\text{int}}+\mathbf{S}_{\text{m}} \\ &= \frac{\phi_{\text{c}}\eta_{\text{c}}}{{}^{t}_{1}\lambda}\int_{\theta_1}\Gamma_1[\mu_\Gamma,\sigma_\Gamma,\theta_1]\left\{\int_1^{{}^{t}_{1}\lambda}\frac{D_1(\mu_0,\sigma_0,{}_0\lambda_{\text{lb}}\,{}_0\lambda_{\text{ub}},{}^{1}_{0}\lambda[\theta_0(\theta_1)],x)}{x}\left(\frac{{}^{t}_{1}\lambda}{x}-1\right)\mathrm{d}x\right\}(\mathbf{n}_0\otimes\mathbf{n}_0)\mathrm{d}\theta_1 \\ &+\phi_{\text{c}}\int_{\alpha}\int_{\beta}\Gamma(\alpha)\Gamma(\beta)\left[d_0 d_1(\lambda_\alpha\lambda_\beta-1)\mathrm{e}^{d_1(\lambda_\alpha\lambda_\beta-1)^2}\left[\frac{\lambda_\beta}{\lambda_\alpha}(\mathbf{n}_0\otimes\mathbf{n}_0)+\frac{\lambda_\alpha}{\lambda_\beta}(\mathbf{m}_0\otimes\mathbf{m}_0)\right]\right]\mathrm{d}\alpha\,\mathrm{d}\beta \\ &+(1-\phi_{\text{c}})(\mu_a(I_1-3)^{a-1}+\mu_b(I_1-3)^{b-1})(\mathbf{I}-C_{33}\mathbf{C}^{-1}).\end{aligned}\right\} \tag{5.3}$$

It is understood that $\mathbf{n}_0$ and $\mathbf{m}_0$ are referred to β_1 and that we merged the Lagrange multiplier with the matrix by assuming a planar tissue to simplify the formulation. This final model has 11 independent fitted parameters $(\eta_{\text{c}}, \mu_\Gamma, \sigma_\Gamma, \mu_0, \sigma_0, a, b, \mu_a, \mu_b, d_0, d_1)$ and three directly determined parameters $(\phi_{\text{c}}, {}_0\lambda_{\text{lb}}, {}_0\lambda_{\text{ub}})$, all with a physical meaning.

5.2. Parameter estimation procedures

While at first glance this appears to be a major nonlinear optimization undertaking with all the usual pitfalls, we can use the following sequence to make actual parameter estimation quite tractable:

(1) From the native tissue mechanical data, predict the collagen phase parameters $(\eta_{\text{c}}, \mu_\Gamma, \sigma\Gamma, \mu_0, \sigma_0)$ using standard procedures [33,63].
(2) From the pre-transition collagen recruitment portion of all of the EXL tissue mechanical data, determine the matrix parameters (a, b, μ_a, μ_b).
(3) Using the ${}^{t}_{1}\mathbf{S}_{\text{c}}(\eta_{\text{c}}, \mu_\Gamma, \sigma_\Gamma, \mu_0, \sigma_0)$ and $\mathbf{S}_{\text{m}}(a, b, \mu_a, \mu_b)$ responses, determine the interaction stress responses for *all test protocols* using $\mathbf{S}_{\text{int}} = \mathbf{S} - \frac{1}{\varphi_{\text{c}}}({}^{t}_{1}\varphi_{\text{c}}\mathbf{S}_{\text{c}} + (1-\varphi_{\text{c}})\mathbf{S}_{\text{m}})$.
(4) Using the results of step 3, determine the final two parameters (d_0, d_1) by fitting equation (5.3) but only allowing them to vary while keeping the other terms to their above-fitted values.

We found that this basic sequence ensured a robust parameter is obtained, because the entire model is never fitted at once. Moreover, this approach allowed us to separate the contributions to the stress of each of these mechanisms. As in our previous studies [33,63], we employed the genetic based Differential Evolution algorithm in Mathematica to perform the optimization. All parameter estimation was performed using a custom program written in Mathematica (Wolfram Research Corp.).

6. Primary results

From the five specimens used, the model was able to successfully fit all data quite well (total fit $r^2 > 0.97$). Moreover, the final parameter values were quite consistent, with generally low standard errors (table 3). The mean collagen fibre modulus (approx. 279 MPa) and fibre splay (approx. 38°) were comparable to previous studies [34]. Interestingly, the lower bound stretch was small (1.01 or approx. 1% strain), so it is likely that it could be set to 1 (i.e. zero strain). The native collagen fibre recruitment parameters were also consistent (table 3), and indicated a very rapid recruitment at stretch of approximately 1.18–1.2 (figure 9). This is a more complete picture of the entire fibre recruitment than in our previous work [8,34], and suggests that the collagen fibres are effectively well ordered with a small deviation in crimp amplitude and wavelength.

One advantage of our approach is that the various contributions to the total stress can be separated (figure 8). To better reveal the present findings, it is useful to examine the effects on the individual stress components under various loading paths. Following the trends of the ensemble results (figure 9), we noted that the interactions produced substantial

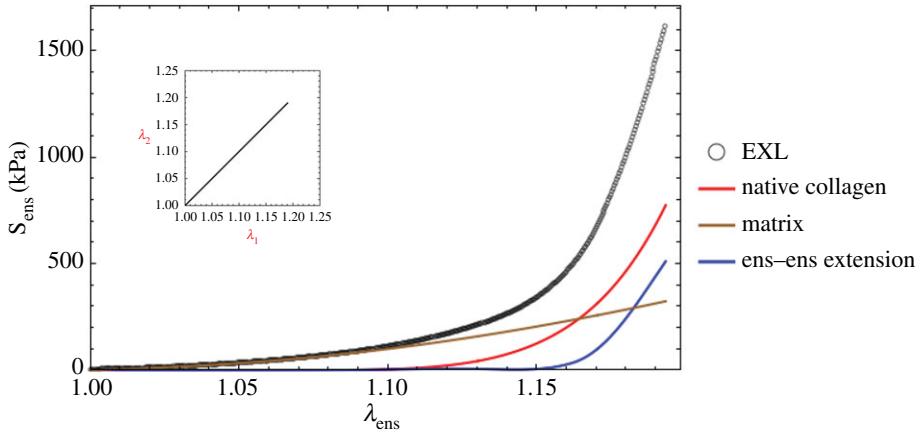

Figure 8. Representative final model results (equation (5.3)) for a single fibre-ensemble stress–strain (in $S_{ens} - \lambda_{ens}$) response for EXL treated bovine pericardium. All model components contributed signficantly to the total stress. Surprisingly, while the collagen phase produced the greatest contribution, the interaction term was of comparable magnitude. (Online version in colour.)

Table 3. Final parameter values for the full model (equation (5.3)) for all five specimens.

	modulus	ODF		recruitment					
	η_c (MPa)	μ_Γ (°)	σ_Γ (°)	μ_D	σ_D	λ_{lb}	λ_{ub}	d_0 (kPa)	d_1
mean	278.94	6.513	38.430	1.185	0.014	1.011	1.197	1.040	42.267
s.e.m.	22.38	1.645	0.922	0.032	0.001	0.007	0.035	0.255	9.772
	matrix								
ID	μ_a (kPa)	a	μ_b (kPa)	b					
mean	56.74	1.068	1294.38	1.873					
s.e.m.	10.69	0.004	340.71	0.007					

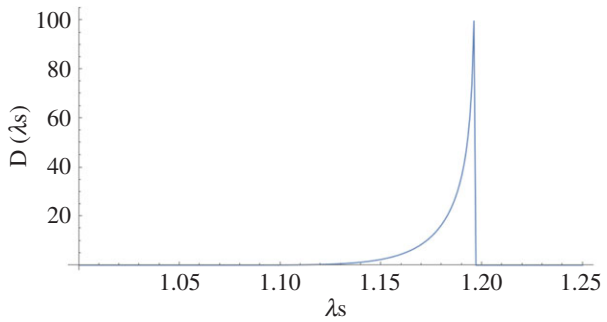

Figure 9. Representative complete collagen fibre recruitment for the pericardial tissue, showing a rapid recruitment near the upper bound, suggesting the collagen fibres have similar crimp geometries in the native state. (Online version in colour.)

contributions to the total stress (figure 10). Interestingly, for S_{11} the interactions actually produced the largest contributions, followed by the matrix and collagen fibres. By contrast, for S_{22} the contributions were much more dependent on the particular loading path, with the collagen phase dominating when $\lambda_2 > \lambda_1$. When $\lambda_1 > \lambda_2$, the matrix phase dominated S_{22}. We further note here that the contribution of the matrix was much less loading path sensitive, due to its near-linear, isotropic behaviour.

7. Discussion

7.1. Major findings

This study represents the first rigorous *full structural model* (i.e. explicitly incorporating various features of the CFA) for cross-linked soft tissues, and also includes a specific interaction term. An important utility of this model is its ability to separate the effects of EXLs on the fibres and matrix, so that the matrix, collagen and interaction effects could be clearly identified. This was made possible, in-part, with the use of the native–EXL matched experimental dataset and a modification to the structural model so that the uncross-linked collagen fibre responses could be mapped to the EXL configuration. As in our previous study, we found that the matrix could be well modelled as an isotropic material. However, we found that a much more linear-like response was necessary. Perhaps the most novel findings of this study were that (i) the effective collagen fibre modulus was unaffected by cross-linking and (ii) the interaction term played such a large role in stress development, often dominating the response (depending on the component and loading path being considered).

The lack of change in the effective collagen fibre modulus has been corroborated by experimental results from Gentleman *et al.* [16]. In that study, they found a modulus range of 269.7 ± 11.9 to 484.7 ± 76.3 for cross-linked collagen fibres in the bovine Achilles tendon, which corresponds to the same

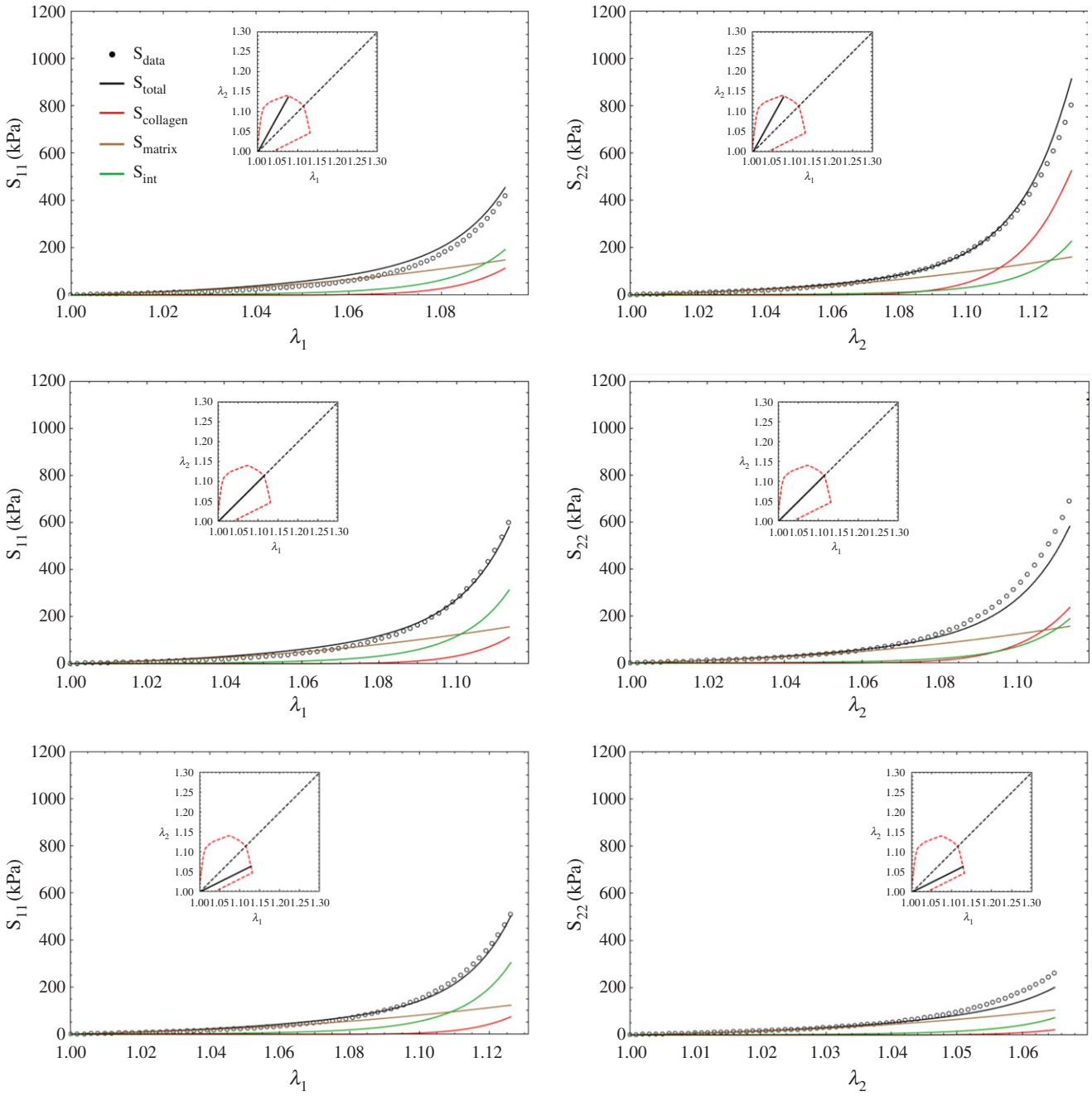

Figure 10. Complete model (equation (5.3)) results for the S_{11} and S_{22} stress components for three protocols. Interestingly for S_{11} the interactions actually produced the largest contributions, followed by the matrix and collagen fibres. By contrast, for S_{22} the contributions were much more dependent on the particular loading path, with the collagen phase dominating when $\lambda_2 > \lambda_1$. When $\lambda_1 > \lambda_2$ the matrix phase dominated S_{22}. We further note here that the contribution of the matrix was much less loading path sensitive, owing to its near-linear, isotropic behaviour. (Online version in colour.)

range as another study for native collagen fibres from various sources [17]. Yang *et al*. [18,64] determined that for the mechanical properties of *hydrated* native and cross-linked type I collagen fibrils that cross-linking the collagen fibrils with a water-soluble carbodiimide did not significantly affect the bending modulus. The work by Shen *et al*. [15] noted a modulus of 0.86 ± 0.45 GPa (range, 0.36–1.60 GPa; $n = 13$), in reasonable agreement with our results. Further, six of the 13 fibrils showed linear behaviour. At the tissue level, our findings are also consistent with the findings of Lee *et al*. [65–67], who found no change in MTM in cross-linked pericardial tissues as in our study (table 2). It is interesting to note that, when using the native tissue fibre-ensemble model (equation (4.4)) on both the native and cross-linked data (figure 5), one can increase the fibre modulus determined from the native state to match the post-EXL data (figure 11*a*). However, this will induce a parallel increase in the MTM of approximately 75% (figure 11*b*), which is inconsistent with the experimental findings (table 2). This is the case even when compensating for the effects of tissue contraction. This simple simulation lends support to the collagen modulus results (figure 5*c*).

Our model results suggest that the major effect of EXL formation was not the formation of a mechanically substantial matrix or stiffening of the collagen fibres, but rather a *dramatically enhanced bonding both within and between fibre ensembles*. Note that our specific interaction term (equation (4.13)) captured the effects of both individual ensemble stretch and relative stretching between ensembles. This is consistent with what is known about GLUT bond formations (figure 1*a*) [22,23,25–27]. Yet, we found that relative

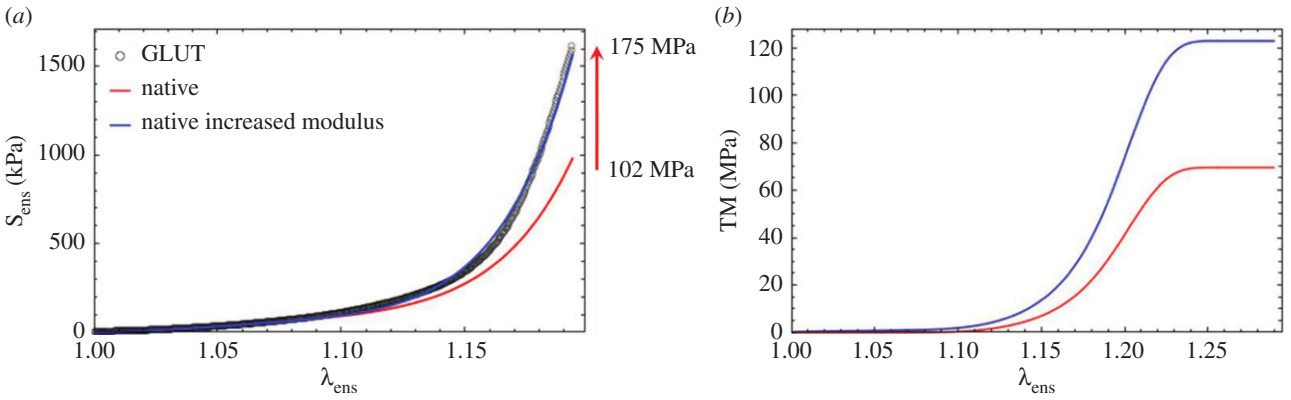

Figure 11. Simulation results using the unmodified native tissue fibre-ensemble model (equation (4.4)) on both the native and cross-linked data from figure 5, showing that one can increase the fibre modulus determined from the native state to match the post-EXL data (*a*). However, this will induce a parallel increase in the MTM of approximately 75% (*b*), which is inconsistent with the experimental findings (table 2). This is the case even when compensating for the effects of tissue contraction. (Online version in colour.)

rotations between fibre ensembles as modelled by equation (4.15) could not capture the observed responses. The underlying structural mechanisms for this behaviour remain largely uncharacterized. One possibility is that the protein core of the proteoglycans that bind collagen fibrils become strongly cross-linked and are thus substantially stiffened, acting to more cohesively bind the collagen fibres. This is supported by findings of Liao & Vesely [68], who observed substantial deformations of proteoglycans in mitral valve chordae under stretch. Moreover, the present model suggests that such mechanisms are strongly associated with fibre-ensemble orientation distributions. While not the final word, our results suggest that EXLs produce a stiffening effect via an isotropic matrix, with the interaction effects being the dominant effect.

7.2. Modelling approach

The present approach was a direct extension of the stochastic, tissue-level meso-structural models first pioneered by Lanir [19] and used in various applications and extensions by our group [8,33,63]. By meso-scale, we refer to the fibre-ensemble scale, which is fibre features down to approximately 100 µm. Moreover, recent evidence has demonstrated that the underlying affine kinematic assumption is valid [34,35], so that the strain energy of each fibre ensemble can be kinematically connected with the macroscopic strain tensor. We took the approach to develop a more general model first, then show what components could be modified or removed entirely. Given the lack of knowledge and modelling efforts in this area, we felt this was appropriate and helped to illustrate what underlying mechanisms should be incorporated. We also considered a more extensive approach based on elastica-based theory for sinusoidal fibres based on [69] under the assumption that EXL formation dramatically increased the fibre modulus, which ultimately proved to be unnecessary. An inter-fibre sliding model was also developed based on the relative sliding between fibres due to differences between their respective slack lengths, and used as a means to model the intra-ensemble EXL effects. However, this approach was found to be unable to capture the individual fibre-ensemble responses, suggesting that relative sliding between fibres at the ensemble level was not a major mechanism. A final question that may impact physical plausibility of the current model is convexity and physical plausibility. Lanir [70] demonstrated that the native tissue structural model is compatible with a physically plausible response. Based on both this and the experimental observations, we focused on monotonically increasing functions of strain for all model terms to ensure physical plausibility and that convexity was maintained.

7.3. Limitations and future directions

The current model is limited in the fact that it is quasi-static and does not account for permanent set phenomena we have observed [71]. The homogenization method used in §3 is fairly standard and has been used by others and the author for some time (e.g. [8,33,34]). We have observed that for soft tissues, whose composition is dominated by a dense network of distinct fibres, especially collagen type I and elastin, these structures can be mechanically treated as fibre ensembles; that is, groups of fibres with a common orientation. The scale of the representative volume element is about 100 µm, which is sufficient to capture the salient mechanical features of the fibre ensemble. We emphasize that this is not meant to be a universal model of all types of soft tissue structures, which are very diverse for a single theoretical treatment. Rather, we focus on a sufficiently generalized approach for exogenously cross-linked dense collagenous tissues, such as pericardium, heart valves and sclera. These structures fit our approach well and also have important biomedical therapeutic applications.

A complete understanding of the current phenomena must be based on well-characterized micro-scale events. For example, Kojic *et al*. [72] developed a model for fibre–fibre kinetics that uses Coulomb friction, which results in a simple and robust approach for tissue simulations. However, our knowledge of even native tissues at the micro-level remains limited. The situation remains more complicated by the fact that our knowledge of the interrelationships between the physical chemistry of EXLs and the macro-scale mechanics of collagenous tissues remains limited at the present time for more sophisticated models to be reliably attempted. To date, no material model is able to fully account for such complex observed microstructural and biological behaviour. The next steps include incorporation of the permanent set effect commonly observed in cross-linked tissues into the present model, and exploration of how alternative cross-linking methods affect macro-scale tissue behaviours.

Authors' contributions. M.S.S. developed the research approach, the analytic approaches and wrote the paper; W.Z. coded the parameter estimation program, reanalysed the experimental data, fitted all data and tabulated results; S.W. assisted with the extension of the native tissue model to handle changes in reference configuration.

Competing interests. We declare we have no competing interests.

Funding. This study was supported by NIH grant no. R01 HL108330.

References

1. Bini A, Mann KG, Kudryk BJ, Schoen FJ. 1999 Noncollagenous bone matrix proteins, calcification, and thrombosis in carotid artery atherosclerosis. *Arterioscler. Thromb. Vasc. Biol*. **19**, 1852–1861. (doi:10.1161/01.ATV.19.8.1852)
2. Schoen FJ. 2005 Cardiac valves and valvular pathology: update on function, disease, repair, and replacement. *Cardiovasc. Pathol*. **14**, 189–194. (doi:10.1016/j.carpath.2005.03.005)
3. Schoen FJ, Levy RJ. 1999 Founder's Award, 25th Annual Meeting of the Society for Biomaterials, perspectives. Providence, RI, April 28-May 2, 1999. Tissue heart valves: current challenges and future research perspectives. *J. Biomed. Mater. Res*. **47**, 439–465. (doi:10.1002/(SICI)1097-4636(19991215)47:4<439::AID-JBM1>3.0.CO;2-0)
4. Vesely I, Barber JE, Ratliff NB. 2001 Tissue damage and calcification may be independent mechanisms of bioprosthetic heart valve failure. *J. Heart Valve Dis*. **10**, 471–477.
5. Sacks MS, Schoen FJ (eds). 1999 *Calcification-independent collagen damage in explanted clinical bioprosthetic heart valves*. Providence, RI: Society for Biomaterials.
6. Schoen FJ, Levy RJ. 2005 Calcification of tissue heart valve substitutes: progress toward understanding and prevention. *Ann. Thorac. Surg*. **79**, 1072–1080. (doi:10.1016/j.athoracsur.2004.06.033)
7. Schoen FJ. 2001 Pathology of heart valve substitution with mechanical and tissue prostheses. In *Cardiovascular pathology* (eds MD Silver, AI Gotlieb, FJ Schoen), pp. 629–677. New York, NY: Livingstone.
8. Sacks MS. 2003 Incorporation of experimentally-derived fiber orientation into a structural constitutive model for planar collagenous tissues. *J. Biomech. Eng*. **125**, 280–287. (doi:10.1115/1.1544508)
9. Sun W, Sacks MS. 2005 Finite element implementation of a generalized Fung-elastic constitutive model for planar soft tissues. *Biomech. Model Mechanobiol*. **4**, 190–199. (doi:10.1007/s10237-005-0075-x)
10. Parry DA. 1988 The molecular and fibrillar structure of collagen and its relationship to the mechanical properties of connective tissue. *Biophys. Chem*. **29**, 195–209. (doi:10.1016/0301-4622(88)87039-X)
11. Gelse K, Poschl E, Aigner T. 2003 Collagens–structure, function, and biosynthesis. *Adv. Drug Deliv. Rev*. **55**, 1531–1546. (doi:10.1016/j.addr.2003.08.002)
12. Petruska JA, Hodge AJ. 1964 A subunit model for the tropocollagen macromolecule. *Proc. Natl Acad. Sci. USA* **51**, 871–876. (doi:10.1073/pnas.51.5.871)
13. Nimni ME. 1988 Biochemistry and biomechanics. In *Collagen volume II biochemistry and biomechanics* (ed. ME Nimni). Boca Raton, FL: CRC Press.
14. Sacks MS, Merryman WD, Schmidt DE. 2009 On the biomechanics of heart valve function. *J. Biomech*. **42**, 1804–1824. (doi:10.1016/j.jbiomech.2009.05.015)
15. Shen ZL, Dodge MR, Kahn H, Ballarini R, Eppell SJ. 2008 Stress-strain experiments on individual collagen fibrils. *Biophys. J*. **95**, 3956–3963. (doi:10.1529/biophysj.107.124602)
16. Gentleman E, Lay AN, Dickerson DA, Nauman EA, Livesay GA, Dee KC. 2003 Mechanical characterization of collagen fibers and scaffolds for tissue engineering. *Biomaterials* **24**, 3805–3813. (doi:10.1016/S0142-9612(03)00206-0)
17. Eppell SJ, Smith BN, Kahn H, Ballarini R. 2006 Nano measurements with micro-devices: mechanical properties of hydrated collagen fibrils. *J. R. Soc. Interface* **3**, 117–121. (doi:10.1098/rsif.2005.0100)
18. Yang L, Fitié CFC, van der Werf KO, Bennink ML, Dijkstra PJ, Feijen J. 2008 Mechanical properties of single electrospun collagen type I fibers. *Biomaterials* **29**, 955–962. (doi:10.1016/j.biomaterials.2007.10.058)
19. Lanir Y. 1983 Constitutive equations for fibrous connective tissues. *J. Biomech*. **16**, 1–12. (doi:10.1016/0021-9290(83)90041-6)
20. Sacks MS, Sun W. 2003 Multiaxial mechanical behavior of biological materials. *Annu. Rev. Biomed. Eng*. **5**, 251–284. (doi:10.1146/annurev.bioeng.5.011303.120714)
21. Cheung DT, Tong D, Perelman N, Ertl D, Nimni ME. 1990 Mechanism of crosslinking of proteins by glutaraldehyde. IV. *In vitro* and *in vivo* stability of a crosslinked collagen matrix. *Connect Tissue Res*. **25**, 27–34. (doi:10.3109/03008209009009810)
22. Nimni ME, Cheung D, Strates B, Kodama M, Sheikh K. 1987 Chemically modified collagen: a natural biomaterial for tissue replacement. *J. Biomed. Mater. Res*. **21**, 741–771. (doi:10.1002/jbm.820210606)
23. Cheung DT, Perelman N, Ko EC, Nimni ME. 1985 Mechanism of crosslinking of proteins by glutaraldehyde. III. Reaction with collagen in tissues. *Connect Tissue Res*. **13**, 109–115. (doi:10.3109/03008208509152389)
24. Gendler E, Gendler S, Nimni ME. 1984 Toxic reactions evoked by glutaraldehyde-fixed pericardium and cardiac valve tissue bioprosthesis. *J. Biomed. Mater. Res*. **18**, 727–736. (doi:10.1002/jbm.820180703)
25. Cheung DT, DiCesare P, Benya PD, Libaw E, Nimni ME. 1983 The presence of intermolecular disulfide cross-links in type III collagen. *J. Biol. Chem*. **258**, 7774–7778.
26. Cheung DT, Nimni ME. 1982 Mechanism of crosslinking of proteins by glutaraldehyde I: reaction with model compounds. *Connect Tissue Res*. **10**, 187–199. (doi:10.3109/03008208209034418)
27. Cheung DT, Nimni ME. 1982 Mechanism of crosslinking of proteins by glutaraldehyde II: reaction with monomeric and polymeric collagen. *Connect Tissue Res*. **10**, 201–216. (doi:10.3109/03008208209034419)
28. Sacks MS. 2000 A structural constitutive model for chemically treated planar tissues under biaxial loading. *Comput. Mech*. **26**, 243–249. (doi:10.1007/s004660000175)
29. Sun W, Sacks MS, Sellaro TL, Slaughter WS, Scott MJ. 2003 Biaxial mechanical response of bioprosthetic heart valve biomaterials to high in-plane shear. *J. Biomech. Eng*. **125**, 372–380. (doi:10.1115/1.1572518)
30. Sacks MS, Chuong CJ. 1998 Orthotropic mechanical properties of chemically treated bovine pericardium. *Ann. Biomed. Eng*. **26**, 892–902. (doi:10.1114/1.135)
31. Sacks MS. 1999 A method for planar biaxial testing that includes in-plane shear. *J. Biomech. Eng*. **121**, 551–555. (doi:10.1115/1.2835086)
32. Zhang W, Feng Y, Lee CH, Billiar KL, Sacks MS. 2015 A generalized method for the analysis of planar biaxial mechanical data using tethered testing configurations. *J. Biomech. Eng*. **137**, 064501. (doi:10.1115/1.4029266)
33. Fata B, Zhang W, Amini R, Sacks M. 2014 Insights into regional adaptations in the growing pulmonary artery using a meso-scale structural model: effects of ascending aorta impingement. *J. Biomech. Eng*. **136**, 021009. (doi:10.1115/1.4026457)
34. Fan R, Sacks MS. 2014 Simulation of planar soft tissues using a structural constitutive model: finite element implementation and validation. *J. Biomech*. **47**, 2043–2054. (doi:10.1016/j.jbiomech.2014.03.014)
35. Lee C-H, Zhang W, Liao J, Carruthers CA, Sacks Jacob I, Sacks Michael S. 2015 On the presence of affine fibril and fiber kinematics in the mitral valve anterior leaflet. *Biophys. J*. **108**, 2074–2087. (doi:10.1016/j.bpj.2015.03.019)
36. Lanir Y. 1979 A structural theory for the homogeneous biaxial stress-strain relationships in flat collageneous tissues. *J. Biomech*. **12**, 423–436. (doi:10.1016/0021-9290(79)90027-7)
37. Sasaki N, Odajima S. 1996 Elongation mechanism of collagen fibrils and force-strain relations of tendon

at each level of structural hierarchy. *J. Biomech.* **29**, 1131–1136. (doi:10.1016/0021-9290(96)00024-3)

38. Sasaki N, Odajima S. 1996 Stress-strain curve and Young's modulus of a collagen molecule as determined by the X-ray diffraction technique. *J. Biomech.* **29**, 655–658. (doi:10.1016/0021-9290(95)00110-7)
39. Liao J, Yang L, Grashow J, Sacks MS. 2005 Molecular orientation of collagen in intact planar connective tissues under biaxial stretch. *Acta Biomater.* **1**, 45–54.
40. Liao J, Yang L, Grashow J, Sacks MS. 2007 The relation between collagen fibril kinematics and mechanical properties in the mitral valve anterior leaflet. *J. Biomech. Eng.* **129**, 78–87. (doi:10.1115/1.2401186)
41. Buehler MJ. 2006 Atomistic and continuum modeling of mechanical properties of collagen: elasticity, fracture, and self-assembly. *J. Mater. Res.* **21**, 1947–1961. (doi:10.1557/jmr.2006.0236)
42. Sacks MS, Mirnajafi A, Sun W, Schmidt P. 2006 Bioprosthetic heart valve heterograft biomaterials: structure, mechanical behavior and computational simulation. *Exp. Rev. Med. Dev.* **3**, 817–834. (doi:10.1586/17434440.3.6.817)
43. Sun W, Abad A, Sacks MS. 2005 Simulated bioprosthetic heart valve deformation under quasi-static loading. *J. Biomech. Eng.* **127**, 905–914. (doi:10.1115/1.2049337)
44. Sellaro TL, Hildebrand D, Lu Q, Vyavahare N, Scott M, Sacks MS. 2007 Effects of collagen fiber orientation on the response of biologically derived soft tissue biomaterials to cyclic loading. *J. Biomed. Mater. Res. A* **80**, 194–205. (doi:10.1002/jbm.a.30871)
45. Alferiev I, Stachelek SJ, Lu Z, Fu AL, Sellaro TL, Connolly JM, Bianco RW, Sacks MS, Levy RJ. 2003 Prevention of polyurethane valve cusp calcification with covalently attached bisphosphonate diethylamino moieties. *J. Biomed. Mater. Res. A* **66**, 385–395. (doi:10.1002/jbm.a.10896)
46. Wells SM, Sellaro T, Sacks MS. 2005 Cyclic loading response of bioprosthetic heart valves: effects of fixation stress state on the collagen fiber architecture. *Biomaterials* **26**, 2611–2619. (doi:10.1016/j.biomaterials.2004.06.046)
47. Wells SM, Sacks MS. 2002 Effects of fixation pressure on the biaxial mechanical behavior of porcine bioprosthetic heart valves with long-term cyclic loading. *Biomaterials* **23**, 2389–2399. (doi:10.1016/S0142-9612(01)00375-1)
48. Wells SM, Sacks MS. 2000 Effects of stress-state during fixation on the fatigue properties of bioprosthetic heart valve tissue. *Trans. Sixth World Biomater. Congress* **2**, 794.
49. Wells SM, Naimark WA, Lee JM. 1999 Thermomechanical characterization of collagen crosslinking in developing cardiovascular tissues. *ASME Adv. Bioeng.* **43**, 91.
50. Lee J, Haberer S, Pereira C, Naimark W, Courtman D, Wilson G. 1994 High strain rate testing and structural analysis of pericardial bioprosthetic materials. In *Biomaterials' mechanical properties. STP 1173* (eds H Kambic, A Yokobori), pp. 19–42. Philadelphia, PA: ASTM.
51. Naimark WA, Lee JM, Limeback H, Cheung D. 1992 Correlation of structure and viscoelastic properties in the pericardia of four mammalian species. *Amer. J. Physiol.* **263**, H1095–H1106.
52. Lee TC, Midura RJ, Hascall VC, Vesely I. 2001 The effect of elastin damage on the mechanics of the aortic valve. *J. Biomech.* **34**, 203–210. (doi:10.1016/S0021-9290(00)00187-1)
53. Barber JE, Ratliff N, Vesely I. 1999 Mechanics of explanted bioprosthetic heart valves. *Biomed. Sci. Instrum.* **35**, 29–32.
54. Mirnajafi A, Raymer J, Scott MJ, Sacks MS. 2005 The effects of collagen fiber orientation on the flexural properties of pericardial heterograft biomaterials. *Biomaterials.* **26**, 795–804. (doi:10.1016/j.biomaterials.2004.03.004)
55. Cavalcante FS *et al.* 2005 Mechanical interactions between collagen and proteoglycans: implications for the stability of lung tissue. *J. Appl. Physiol.* **98**, 672–679. (doi:10.1152/japplphysiol.00619.2004)
56. Coughlin MF, Suki B, Stamenovic D. 1996 Dynamic behavior of lung parenchyma in shear. *J. Appl. Physiol.* **80**, 1880–1890.
57. Grashow JS, Sacks MS, Liao J, Yoganathan AP. 2006 Planar biaxial creep and stress relaxation of the mitral valve anterior leaflet. *Ann. Biomed. Eng.* **34**, 1509–1518. (doi:10.1007/s10439-006-9183-8)
58. Sacks MS. 2006 Biaixal stress-stretch behavior of the mitral valve anterior leaflet at physiologic strain rates. *Ann. Biomed. Eng.* **34**, 315–325. (doi:10.1007/s10439-005-9027-y)
59. Stella JA, Liao J, Sacks MS. 2007 Time-dependent biaxial mechanical behavior of the aortic heart valve leaflet. *J. Biomech.* **40**, 3169–3177. (doi:10.1016/j.jbiomech.2007.04.001)
60. Eckert CE, Fan R, Mikulis B, Barron M, Carruthers CA, Friebe VM, Vyavahare NR, Sacks MS. 2013 On the biomechanical role of glycosaminoglycans in the aortic heart value leaflet. *Acta Biomat.* **9**, 4653–4660. (doi:10.1016/j.actbio.2012.09.031)
61. Holzapfel GA. 2000 *Nonlinear solid mechanics: a continuum approach for engineering*. Chichester, NY: Wiley.
62. Merodio J, Ogden RW. 2006 The influence of the invariant I-8 on the stress-deformation and ellipticity characteristics of doubly fiber-reinforced non-linearly elastic solids. *Int. J. Non-Linear Mech.* **41**, 556–563. (doi:10.1016/j.ijnonlinmec.2006.02.001)
63. Zhang W, Ayoub S, Liao J, Sacks MS. In press. On the mechanical role of collagen and elastin fibers in the layers of the mitral heart valve leaflet. *J. Mech. Behav. Biomed. Mater.*
64. Yang L, van der Werf KO, Koopman BFJM, Subramaniam V, Bennink ML, Dijkstra PJ, Feijen J. 2007 Micromechanical bending of single collagen fibrils using atomic force microscopy. *J. Biomed. Mater. Res. A* **82A**, 160–168. (doi:10.1002/jbm.a.31127)
65. Lee JM, Corrente R, Haberer SA. 1989 The bovine pericardial xenograft. II. Effect of tethering or pressurization during fixation on the tensile viscoelastic properties of bovine pericardium. *J. Biomed. Mater. Res.* **23**, 477–489. (doi:10.1002/jbm.820230503)
66. Lee JM, Haberer SA, Boughner DR. 1989 The bovine pericardial xenograft. I. Effect of fixation in aldehydes without constraint on the tensile viscoelastic properties of bovine pericardium. *J. Biomed. Mater. Res.* **23**, 457–475. (doi:10.1002/jbm.820230502)
67. Lee JM, Ku M, Haberer SA. 1989 The bovine pericardial xenograft. III. Effect of uniaxial and sequential biaxial stress during fixation on the tensile viscoelastic properties of bovine pericardium. *J. Biomed. Mater. Res.* **23**, 491–506. (doi:10.1002/jbm.820230504)
68. Liao J, Vesely I. 2004 Relationship between collagen fibrils, glycosaminoglycans, and stress relaxation in mitral valve chordae tendineae. *Ann. Biomed. Eng.* **32**, 977–983. (doi:10.1023/B:ABME.0000032460.97278.e9)
69. Garikipati K, Göktepe S, Miehe C. 2008 Elastica-based strain energy functions for soft biological tissue. *J. Mech. Phys. Solids* **56**, 1693–1713. (doi:10.1016/j.jmps.2007.07.005)
70. Lanir Y. 1994 Plausibility of structural constitutive-equations for isotropic soft-tissues in finite static deformations. *J. Appl. Mech.-T Asme* **61**, 695–702. (doi:10.1115/1.2901516)
71. Sun W, Sacks M, Fulchiero G, Lovekamp J, Vyavahare N, Scott M. 2004 Response of heterograft heart valve biomaterials to moderate cyclic loading. *J. Biomed. Mater. Res.* **69A**, 658–669. (doi:10.1002/jbm.a.30031)
72. Kojic M, Mijailovic S, Zdravkovic N. 1998 A numerical algorithm for stress integration of a fiber-fiber kinetics model with Coulomb friction for connective tissue. *Comput. Mech.* **21**, 189–198. (doi:10.1007/s004660050294)